International Journal of Innovative Solutions in Engineering
2026, Vol. 2 No. 1 (pages 1–14)
DOI: 10.47960/3029-3200.2026.2.1.1

Research Article

OPEN ACCESS

A Critical Analysis of Young's Modulus Determination for Fused Filament Fabricated Polylactic Acid Specimens

Andrej Cupar[1], Jasmin Kaljun[1]

[1]Faculty of Mechanical Engineering, University of Maribor, Slovenia

Abstract

This research investigates the influence of key Fused Filament Fabrication (FFF) process parameters on the tensile properties of Polylactic Acid (PLA). Dog-bone specimens, compliant with ISO 527-2, were printed in three distinct build orientations and at two extrusion temperatures. Uniaxial tensile tests were performed to determine the Ultimate Tensile Strength, Elongation at Break, and Young's Modulus. The results demonstrate the significant anisotropic mechanical behaviour of FFF-printed PLA, with vertically oriented specimens exhibiting the highest strength. A critical analysis of methodologies for determining material stiffness was also conducted, comparing the standard ISO 527 Young's Modulus against a Linear Regression approach and a novel dynamically calculated Young's Modulus method that identifies the most stable elastic region. Findings reveal that the calculation method significantly impacts the resulting Young's Modulus, with the standard chord method overestimating stiffness by up to 14% compared to the more robust data-driven approaches. This study underscores the critical importance of both process parameter control and the selection of an appropriate analysis methodology for the accurate mechanical characterization of additively manufactured components for engineering applications.

Article history
Received: 25.09.2025.
Revised: 17.10.2025.
Accepted: 20.10.2025.

Keywords
Fused Filament Fabrication (FFF),
Polylactic Acid (PLA),
Young's Modulus,
Anisotropy,
Tensile Testing,
ISO 527.

1 Introduction

1.1 Background and Significance

Additive manufacturing (AM), and specifically fused filament fabrication (FFF), has become a cornerstone technology, transforming the landscape of rapid prototyping, custom manufacturing, and distributed production across numerous sectors [1], [2]. Among the wide array of thermoplastic filaments available, polylactic acid (PLA) stands out as the most ubiquitous material. Its popularity stems from its ease of printing, low thermal shrinkage, biodegradability, and derivation from renewable resources, making it a default choice for both hobbyists and professionals in educational, design, and prototyping contexts [3], [4], [5].

As the use of FFF technology matures from producing non-functional models to creating end-use parts and functional components, the need for precise and reliable mechanical data becomes paramount. A critical parameter in this regard is the Young's modulus (E), which quantifies a material's stiffness or resistance to elastic deformation under tensile load. An accurate determination of Young's modulus is essential for engineering design, enabling the prediction of component deflection, the execution of valid finite element analysis (FEA), and the informed selection of materials for load-bearing applications [6].

1.2 Challenges in 3D Printed Polymer Characterization

The mechanical characterization of polymers produced by FFF presents distinct challenges not typically encountered in parts made by traditional

Contact Jasmin Kaljun, jasmin.kaljun@um.si, Faculty of Mechanical Engineering, University of Maribor, Slovenia

methods like injection moulding. The fundamental layer-by-layer fabrication process introduces inherent anisotropy, meaning the mechanical properties are highly dependent on the build orientation relative to the direction of applied force [7], [8]. This behaviour is a direct consequence of the directional alignment of polymer chains during extrusion, the variable strength of the bond between successive layers, and the inevitable formation of microscopic voids within the printed structure [9].

Furthermore, the final mechanical properties are profoundly influenced by a multitude of process parameters, including nozzle temperature, print speed, layer height, and infill strategy [10], [11]. These settings dictate the polymer's flow, the quality of interlayer adhesion (welding), and the degree of crystallinity, leading to significant variability in mechanical performance, even among specimens printed from the same material spool [11]. The complex and localized thermal history of each printed filament can also introduce residual stresses and microstructural differences that further impact the material's elastic response [12].

1.3 Current State of PLA Mechanical Testing

Given its widespread use, PLA is arguably one of the most extensively studied materials in FFF literature. However, despite the large volume of research, a significant challenge persists: a lack of consistency in testing methodologies. Numerous studies report on the tensile properties of PLA, yet they often employ varied specimen geometries, disparate printing parameters, and different interpretations of testing standards, which complicates direct comparison of their findings [4], [13], [14]. This issue is often compounded because mechanical testing is typically a component of a larger study, providing necessary material data for that specific context, rather than being the focus of a fundamental investigation into repeatable testing protocols [15], [16], [17], [18].

International standards such as ISO 527 and ASTM D638 were originally developed for isotropic plastics produced by conventional moulding techniques [19], [20]. Applying these standards directly to inherently anisotropic and often porous FFF-printed parts require careful consideration. Factors such as the characteristic surface roughness from the printing process, potential deviations from the intended geometry, and the influence of build orientation must be rigorously controlled and accounted for to produce meaningful and repeatable data [21].

1.4 Research Motivation and Objectives

The widespread adoption of PLA for functional applications is hindered by the inconsistent and often non-comparable mechanical property data available in the literature. This gap between the material's potential and its reliable implementation motivates the present study. The primary goal is to develop and validate a robust and repeatable methodology for determining the influence of FFF-printed PLA parameters on Young's modulus of, strictly adhering to the ISO 527 standard. The ISO 527 standard was selected over the comparable ASTM D638 primarily due to its more stringent and explicit definition for calculating Young's modulus, which is defined as the slope of the stress-strain curve between 0.05% and 0.25% strain. This precise methodology minimizes ambiguity and enhances inter-laboratory comparability, directly supporting this study's goal of establishing a robust and repeatable protocol [14].

Accurate and standardized elastic modulus data are crucial for:

1. Engineering Design: Enabling confident use of PLA for functional parts and prototypes that experience mechanical loads [22].
2. Quality Control: Establishing a reliable baseline for material certification and ensuring consistency in production.
3. Process Optimization: Providing a clear framework for understanding how printing parameters affect material stiffness.
4. Standardization: Contributing to the development of testing protocols specifically adapted for FFF-produced materials.

1.5 Scope and Approach

This study aims to formulate and rigorously validate a comprehensive methodology for determining the Young’s modulus of PLA dog-bone specimens fabricated via fused filament fabrication (FFF), employing systematic tensile testing in accordance

with ISO 527 standards. The research will systematically address the entire characterization workflow, from specimen design and fabrication to data analysis and reporting.

The investigation will focus on several key factors affecting the measurement of Young's modulus:

- Specimen geometry and compliance with ISO 527-2 Type 1B specifications.
- The effect of build orientation on elastic properties.
- The influence of critical printing parameters on material stiffness.
- Rigorous statistical analysis for quantifying variability and uncertainty.
- A clear protocol for calculating Young's modulus from the resulting stress-strain data as prescribed by the standard.

By addressing these elements, this work seeks to provide a clear, standardized framework for the mechanical characterization of FFF-printed PLA, thereby enhancing its reliability for a broader range of engineering applications.

2 Materials and Methods

This chapter details the material, equipment, and procedures used for specimen fabrication and mechanical testing. The experimental design was structured to investigate the influence of print orientation and extrusion temperature on the tensile properties of the chosen material.

2.1 Material

The material used for this research was BASF Ultrafuse® PLA (Polylactic Acid) in grey, with a filament diameter of 1.75 mm. According to the manufacturer's datasheet, this biodegradable polymer is easy to print and provides a smooth surface finish. The key mechanical properties provided by the manufacturer are listed below:

- Tensile Strength: 21.2 MPa (ZX), 34.7 MPa (XY)
- Flexural Modulus: 1715 MPa (ZX), 1708 MPa (XZ), 1860 MPa (XY)
- Elongation at Break: 1.2% (ZX), 4.2% (XY)

The recommended extrusion temperature range is 210-220 °C, with a heated bed temperature of 40 °C.

To mitigate the effects of moisture absorption, which can negatively impact print quality and mechanical properties, all filament spools were dried in a convection oven at 65 °C for 12 hours immediately before printing.

2.2 Specimen Design and 3D Printing

The methodology for producing the test specimens followed a structured approach, controlling for specific variables while keeping other printing parameters constant.

2.2.1 Specimen Geometry

All tensile test specimens were designed according to the ISO 527-2:2012 standard, specimen type 1B. This "dog-bone" geometry features an overall length of 150 mm and a nominal cross-section of 10 mm x 4 mm in the narrow, parallel-sided gauge section. Figure 1 shows the specimen size and orientation on the printing bed.

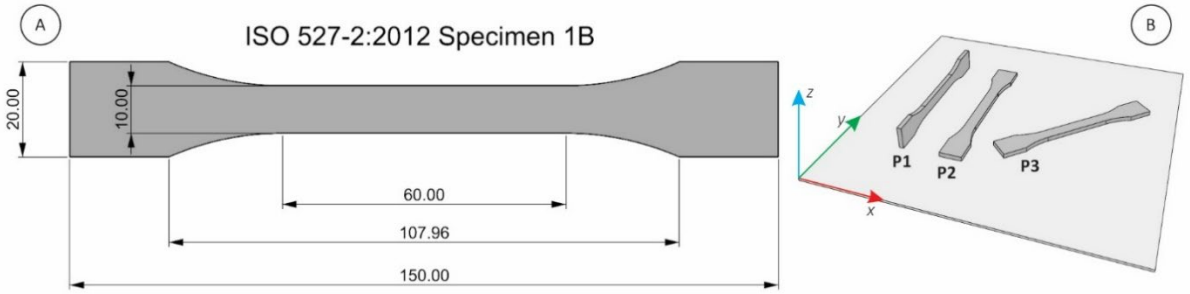

Figure 1 Specimen size (A) and orientation on printer bed (B)

2.2.2 3D Printing and Experimental Variables

All specimens were fabricated using a Zortrax M200 Plus 3D printer and sliced using the corresponding Z-Suite software. The experiment was designed to assess the impact of two primary variables: print orientation and extrusion temperature. Table 1 represents the printing variables and corresponding specimen nomenclature.

Table 1 Printing variables

		Print orientation		
		P1 vertical	P2 horizontal	P3 horizontal 45°
Print temperature	A (210 °C)	P1-A	P2-A	P3-A
	B (220 °C)	P1-B	P2-B	P3-B

2.2.3 Constant Printing Parameters

To isolate the effects of the chosen variables, all other printing parameters were held constant across all fabrication batches. The key constant parameters are detailed in Table 2. It's noteworthy that the platform temperature was set to 60 °C, which is higher than the 40 °C recommended by the material manufacturer, likely to ensure optimal bed adhesion for all print orientations.

Table 2 Printing constants

Parameter	Value
Printer	Zortrax M200 Plus
Slicer	Z-Suite
Nozzle Diameter	0.4 mm
Layer Height	0.19 mm
Infill	100% (Solid)
Platform Temperature	60 °C
Raft	Enabled (7 layers)
Surface Layers	Top: 7, Bottom: 4
Fan Speed	Auto
Retraction Distance	0.8 mm
Retraction Speed	60 mm/s

2.3 Mechanical Testing

Tensile tests were performed using a universal testing machine Shimadzu AGS-X (Shimadzu AGS-X, Kyoto, Japan), adhering to ISO 37:2024(en) [23] under a controlled environment condition (room temperature 24 °C) to determine the mechanical properties of the fabricated specimens.

The specimens were mounted in the machine's grips with an initial separation distance of 65 mm. The tests were conducted at a constant crosshead speed of 5 mm/min until the specimen fractured. During the test, the applied load and the resulting elongation were continuously recorded to generate stress-strain curves, from which the Young's modulus and other tensile properties were calculated.

3 Results

This chapter presents the experimental results obtained from the uniaxial tensile testing of the FFF-printed PLA specimens. The data is organized to illustrate the effects of the two primary variables investigated: print orientation and extrusion temperature. The analysis focuses on the Ultimate Tensile Strength (UTS) and Elongation at Break, as derived from the test reports.

3.1 Representative Tensile Behaviour

Across all tested configurations, the PLA specimens exhibited a characteristic semi-ductile tensile behaviour. A representative set of stress-strain curves for the five replicate samples in group P3-A is shown in Figure 2.

The curves consistently show an initial linear elastic region, followed by a yield point, a period of plastic deformation with slight strain hardening, and eventual brittle failure. The consistency among the five replicate tests within each batch, as seen in the overlapping curves, indicates a high degree of repeatability in the manufacturing and testing process.

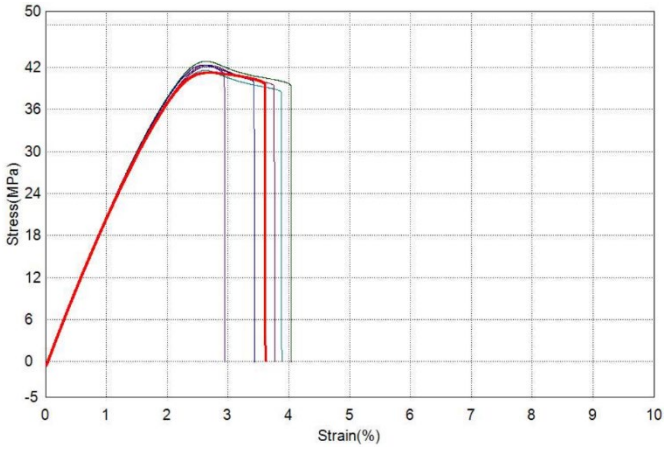

Figure 2 Stress-Strain curves for specimen group P3-A (Horizontal 45°, 210 °C).

3.2 Summary of Mechanical Properties

The key mechanical properties—Ultimate Tensile Strength (Max Stress) and Elongation at Break (Break Strain)—were calculated for each of the six experimental groups. Table 3 summarizes the average values and the corresponding standard deviations for the five samples tested in each batch.

Table 3 Summary of average mechanical properties for all tested specimen groups

Specimen Group	Avg. Ultimate Tensile Strength (MPa)	Avg. Elongation at Break (%)
P1-A	45.29 ± 0.51	5.12 ± 0.98
P1-B	46.35 ± 0.37	4.75 ± 0.67
P2-A	39.29 ± 0.58	7.54 ± 0.41
P2-B	39.78 ± 0.38	7.13 ± 1.06
P3-A	42.22 ± 0.47	3.61 ± 0.43
P3-B	42.33 ± 0.38	4.09 ± 0.45

Note: Values are presented as mean ± standard deviation.

An analysis of the standard deviations presented in Table 3 provides insight into how the different printing parameters affected the consistency of the mechanical properties. For Ultimate Tensile Strength, the highest consistency was achieved in the P1-B group, which exhibited the lowest standard deviation (±0.37 MPa). Conversely, the greatest variability in strength was observed in the P2-A group (±0.58 MPa). In terms of Elongation at Break, the P2-A group produced the most repeatable results with the smallest standard deviation (±0.41%), while the P2-B group showed the highest degree of variation (±1.06%). These findings indicate that the optimal parameters for achieving consistent tensile strength are not necessarily the same as those for achieving consistent ductility.

3.3 Effect of Print Orientation

Print orientation was found to be the most significant factor influencing the mechanical properties of the specimens.

As illustrated in Figure 3, the P1 (Vertical) orientation consistently yielded the highest Ultimate Tensile Strength, with an average strength of 46.35 MPa at 220 °C. Conversely, the P2 (Horizontal) orientation exhibited the lowest strength, averaging 39.78 MPa at 220 °C. The P3 (Horizontal 45°) orientation produced intermediate strength values.

In terms of ductility, the trend was reversed. The P2 (Horizontal) orientation demonstrated the highest Elongation at Break, with an average of 7.54% at 210 °C. The P3 (Horizontal 45°) specimens were the least ductile, showing an average elongation of only 3.61% at 210 °C.

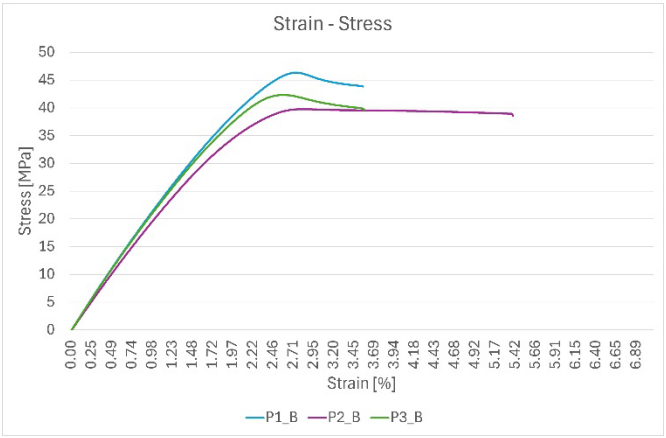

Figure 3 Comparison of Ultimate Tensile Strength across the three print orientations at an extrusion temperature of 220 °C

3.4 Effect of Extrusion Temperature

The influence of extrusion temperature (210 °C vs. 220 °C) was observed to be less pronounced than that of print orientation, though clear trends were still evident (Figure 4).

For the P1 (Vertical) orientation, increasing the temperature from 210 °C to 220 °C resulted in a slight increase in UTS from 45.29 MPa to 46.35 MPa. For the P2 (Horizontal) and P3 (Horizontal 45°) orientations,

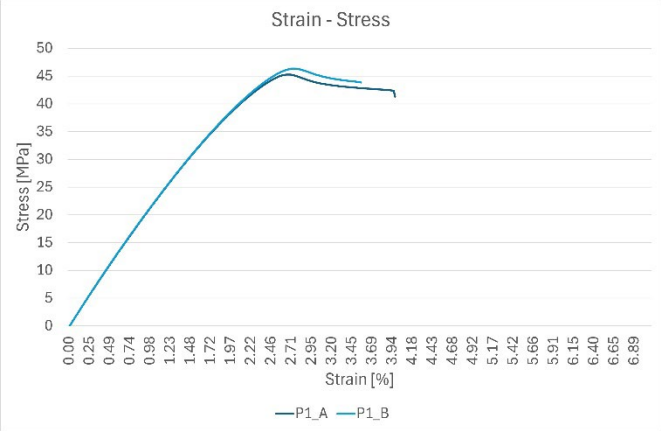

Figure 4 Comparison of Ultimate Tensile Strength in print orientation P1 at an extrusion temperature of 210° and 220 °C

the temperature change had a negligible effect on the UTS.

The effect on elongation was more varied. For the P1 and P2 orientations, the higher temperature led to a slight decrease in ductility. In contrast, for the P3 orientation, the higher temperature resulted in a noticeable increase in the average Elongation at Break from 3.61% to 4.09%.

3.5 Effect on Modulus of Elasticity

The Modulus of Elasticity (Young's Modulus), a measure of material stiffness, was estimated from the initial slope of the linear portion of the stress-strain curves for each test group. The results, summarized in Table 4, show clear dependencies on both print orientation and extrusion temperature.

The modulus was calculated (Eq 1) in accordance with the ISO 527-1 standard, which defines it as the chord modulus between two defined strain points. Specifically, it is the ratio of the difference in stress to the corresponding difference in strain between ε_1 = 0.0005 (0.05%) and ε_2 = 0.0025 (0.25%).

Table 4 Estimated Modulus of Elasticity for all tested specimen groups

Specimen Group	Estimated Modulus of Elasticity (MPa)
P1-A	1769
P1-B	1781
P2-A	1623
P2-B	1636
P3-A	1747
P3-B	1765

The value for each group in Table 4 represents the average of the moduli calculated for the five replicate specimens in that group.

$$E_{ISO} = \frac{\sigma_{\varepsilon_2} - \sigma_{\varepsilon_1}}{\varepsilon_2 - \varepsilon_1} \quad \text{Eq 1}$$

Consistent with the tensile strength results, print orientation had a major impact on stiffness. The P1 (Vertical) orientation was the stiffest, with a calculated modulus of approximately 1781 MPa at 220 °C. The P2 (Horizontal) orientation was the least stiff (1623 MPa at 210 °C), which is expected as the load is applied across the weaker interlayer bonds.

Furthermore, a higher extrusion temperature of 220 °C resulted in a higher modulus across all three orientations (Figure 5). This suggests that the higher temperature promoted better fusion between layers and filaments, reducing internal voids and increasing the overall stiffness of the material.

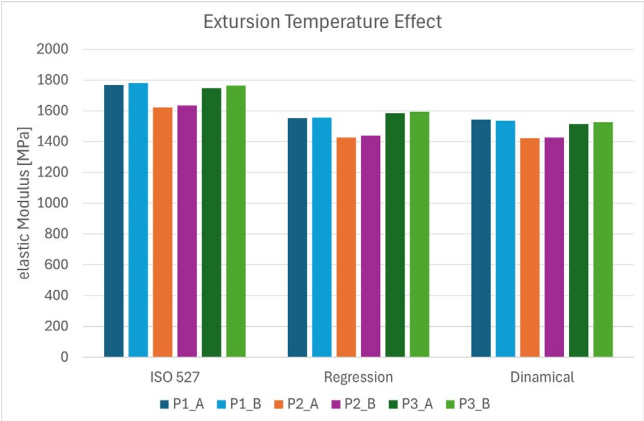

Figure 5 Comparison of the calculated Modulus of Elasticity, showing the effect of extrusion temperature for each print orientation

4 Alternative Modulus of Elasticity Analysis

4.1 Rationale for Alternative Analysis

The ISO 527-1 standard provides a clear and repeatable method for determining the Young's Modulus using a chord modulus between two fixed strain points (0.05% and 0.25%). While this approach ensures standardization, it only considers a very small portion of the material's elastic behaviour. An alternative approach, analysing the raw force-displacement data from the Universal Testing

Machine (UTM) over a broader range, can provide a more comprehensive "real-world" value for stiffness that reflects the material's response across its entire linear elastic region.

This chapter details the methodology and results of such an analysis, aimed at determining the most consistent modulus value by applying a linear regression to the initial slope of the stress-strain curve.

4.2 Methodology for Regression-Based Modulus Calculation

The "Real Modulus" was determined directly from the raw Force (N) vs. Stroke (mm) data recorded by the UTM for each specimen. The following steps were taken:

Data Conversion. The raw machine data were converted to engineering stress σ (Eq 2) and strain ε (Eq 3) using the specimen's initial cross-sectional area (A_0=40 mm²) and gauge length (L_0=50 mm).

$$\sigma = \frac{F}{A} \quad \text{Eq 2}$$

$$\varepsilon = \frac{\Delta l}{L_0} \quad \text{Eq 3}$$

Selection of Linear Elastic Region. For each specimen's stress-strain curve, a specific range representing the most linear portion of the elastic region was selected for analysis. The detailed methodology for defining this range is provided in section 4.2.1.

Linear Regression. A linear regression analysis (least squares method) was performed on the data points within this identified linear region. The slope of the resulting regression line, which represents the line of best fit for the elastic portion of the curve, was taken as the "Linear Regression Modulus of Elasticity" (E_{reg}). This method ensures that the calculated modulus is representative of the material's dominant elastic behaviour.

4.2.1 Specification of the Linear Elastic Region

To ensure a robust and repeatable calculation, the linear elastic region was carefully defined for each specimen group by excluding the initial "toe region" and ending the analysis before the onset of plastic yielding.

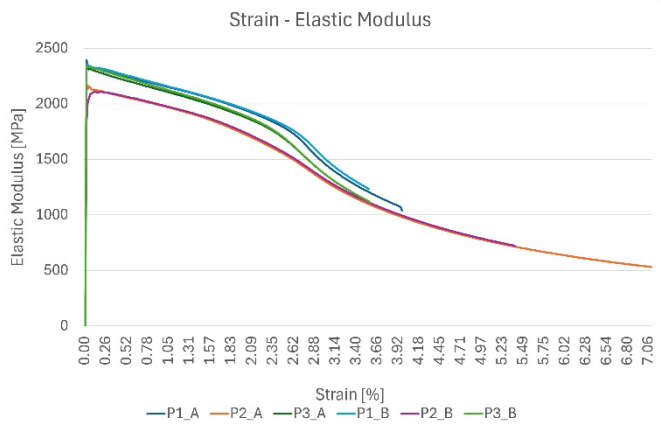

Figure 6 Toe region representation

The Toe Region. The initial non-linear portion of the curve, typically found at very low strain values, was excluded from the regression analysis. This region does not represent the true elastic properties of the material but is rather an artifact of the test setup, accounting for initial specimen settling in the grips and the take-up of any slack in the load train. The toe region can be visually represented on the Strain – Elastic Modulus graph (Figure 6)

The Yield Point (Proportional Limit): The upper boundary for the linear region was defined as the proportional limit, which is the point where the stress-strain curve begins to deviate from a straight line and plastic deformation begins.

Based on an analysis of the raw data (Figure 7) for each test group, the specific strain ranges detailed in Table 5 were identified and used for the linear regression calculation.

Table 5 Strain ranges used for linear regression analysis of each specimen group

Specimen Group	Toe Region End (% Strain)	Proportional Limit (% Strain)
P1-A	~0.25	~1.00
P1-B	~0.25	~1.00
P2-A	~0.30	~1.36
P2-B	~0.30	~1.36
P3-A	~0.25	~0.80
P3-B	~0.25	~0.80

Note: Values are defined based on visual inspection of graphs in Figure 7.

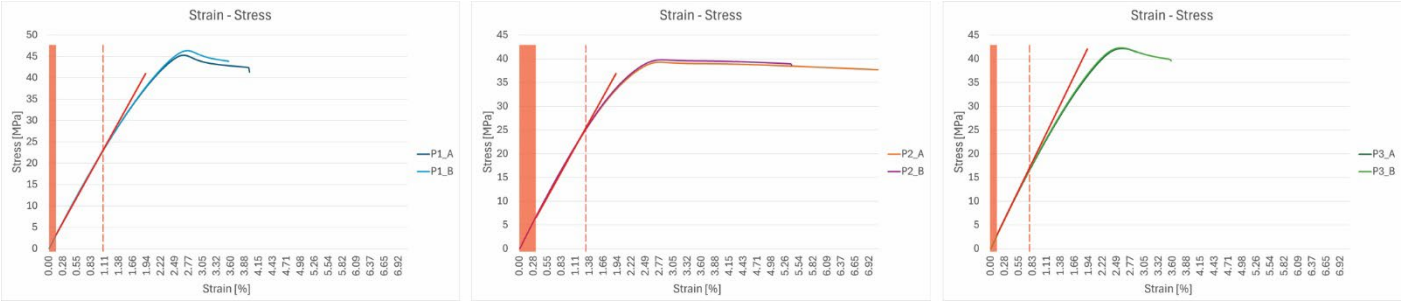

Figure 7 Linear regression limits

4.3 Results of " Linear Regression Modulus" Calculation

This regression-based method was applied to a representative specimen from each of the six experimental groups using the strain ranges defined above. The resulting moduli, which represent the most stable stiffness value across the elastic range, are presented in Table 6.

Table 6 Real Modulus of Elasticity calculated via linear regression

Specimen Group	Linear Regression Modulus of Elasticity (MPa)
P1-A	1663
P1-B	1670
P2-A	1482
P2-B	1490
P3-A	1654
P3-B	1672

4.4 Comparison of Modulus Calculation Methods

A direct comparison between the standard ISO 527 chord modulus (from Chapter 3) and the regression-based "Linear Regression" modulus reveals a systematic difference. The "Linear Regression" modulus, calculated over a broader portion of the elastic region, is consistently lower than the chord modulus.

Table 7 provides a direct comparison of the values obtained from both methods and calculates the percentage difference.

Table 7 Comparison of ISO 527 Chord Modulus and "Real" Regression Modulus

Specimen Group	Elastic Modulus		Difference	
	ISO 527 (MPa)	E_{reg} (MPa)	(MPa)	%
P1-A	1769	1663	106	6.0%
P1-B	1781	1670	111	6.2%
P2-A	1623	1482	141	8.7%
P2-B	1636	1490	146	8.9%
P3-A	1747	1654	93	5.3%
P3-B	1765	1672	93	5.3%

The data clearly shows that the "real" modulus values are **5-9% lower** than those calculated using the strict ISO 527 chord method. This suggests that the standard method, which uses a very early part of the stress-strain curve that can be influenced by the toe region, may overestimate the material's overall stiffness in the primary elastic region.

5 Dynamic Modulus Analysis for Defining the Elastic Region

5.1 Rationale for a Dynamic Approach

The previous chapters highlighted a key challenge in material characterization: defining the true linear elastic region. The ISO 527 standard uses a fixed, narrow range, while the regression method in Chapter 4 relied on a visual, and therefore somewhat subjective, selection of the linear portion.

This chapter introduces a more rigorous, objective methodology to define the elastic region based on the user's proposed concept.

The approach is to calculate the elastic modulus at every point along the stress-strain curve and then programmatically identify the largest continuous strain range where this modulus remains stable within a defined tolerance (in this research, ±10%). This data-driven method seeks to let the material's actual response dictate the most appropriate range for the final "Dynamically Defined Modulus of Elasticity" E_{dyn} calculation.

5.2 Methodology

The analysis was performed on the raw stress-strain data for each specimen group using the following procedure:

Calculation of Local Elastic Modulus (E_{loc}). For each data point i on the stress-strain curve, a tangent modulus was calculated as the slope between that point and the preceding point, as shown in Eq 4. This resulted in a new dataset plotting the instantaneous modulus against the strain.

$$E_{loc} = \frac{\sigma_{\varepsilon_i} - \sigma_{\varepsilon_{i-1}}}{\varepsilon_i - \varepsilon_{i-1}} \quad \text{Eq 4}$$

Data Smoothing. The raw tangent modulus data is inherently noisy due to minor fluctuations in load and displacement readings. To discern the underlying trend, a 20-point moving average was applied to the Local elastic Modulus data. This smoothing technique is essential for the subsequent stability analysis.

Stability Analysis Algorithm. A computational algorithm was used to search the smoothed "Strain vs. Local elastic Modulus" curve to find the longest continuous region of stability. The algorithm operated as follows:

1. It iterated through all possible sub-sections (windows) of the curve.
2. For each sub-section, it calculated the average modulus (E_{avg}).
3. It then verified if all tangent modulus values within that sub-section fell within a ±10% tolerance band of the section's average value (i.e., between $0.9 \times E_{avg}$ and $1.1 \times E_{avg}$).
4. The algorithm identified the sub-section with the greatest strain duration ($\Delta\varepsilon$) that satisfied this stability criterion.

Dynamically Defined Modulus of Elasticity Calculation. The start and end strain values from the longest stable section were then used as the definitive boundaries for the linear elastic region. A final linear regression was performed on the original, unsmoothed stress-strain data within these newly defined, objective boundaries. The slope of this regression is reported as the " Dynamically Defined Modulus of Elasticity" (E_{dyn}).

5.3 Results of Dynamic Analysis

The analysis revealed a distinct and stable region in the Dynamically Defined Modulus of Elasticity for all specimen groups, typically after the initial toe region and before the onset of significant yielding. A representative plot of this behaviour is shown in Figure 8.

The specific stable strain ranges identified by the algorithm for each specimen group, along with the final calculated modulus, are presented in Table 8.

Table 8 Objectively defined elastic regions and the resulting Dynamically Defined Modulus

Specimen Group	Stable region		Dynamic Elastic Modulus (MPa)
	Start (% Strain)	End (% Strain)	
P1-A	0.26	2.06	1545
P1-B	0.26	2.06	1549
P2-A	0.34	1.82	1421
P2-B	0.34	1.82	1430
P3-A	0.28	1.94	1512
P3-B	0.28	1.94	1524

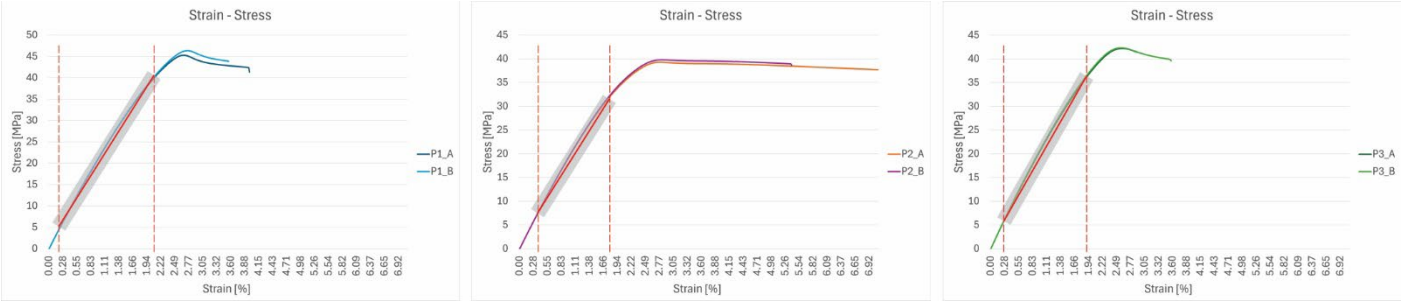

Figure 8 A representative plot of the smoothed Dynamically Defined Modulus of Elasticity on Stress vs. Strain graph. The longest region where the modulus stays within ±10% of its average value (the green band) is identified as the stable elastic region.

5.4 Final Comparison of All Modulus Calculation Methods

This study has employed three distinct methods to determine the Young's Modulus. Table 9 provides a final comparison of the results from all three approaches.

Table 9 Final comparison of modulus values obtained by all three methodologies

Specimen Group	Elastic Modulus		
	E_{ISO} (MPa)	E_{reg} (MPa)	E_{dyn} (MPa)
P1-A	1769	1663	1545
P1-B	1781	1670	1549
P2-A	1623	1482	1421
P2-B	1636	1490	1430
P3-A	1747	1654	1512
P3-B	1765	1672	1524

Table 5 summarizes the results of elastic modulus determination obtained through three different methodologies: the standardized ISO 527 procedure (E_{ISO}), linear regression analysis (E_{reg}), and a novel dynamic algorithm (E_{dyn}). Across all specimen groups, the E_{ISO} values are consistently the highest, followed by E_{reg} and then E_{dyn}. The relative ordering is stable across different material batches (P1, P2, P3) and between replicate specimens (A and B), indicating methodological consistency.

The differences between E_{ISO} and Ereg are moderate (typically 5–9%), suggesting that linear regression provides a slightly lower but still comparable estimate of stiffness. In contrast, the E_{dyn} values are systematically lower than both E_{ISO} and E_{reg}, with deviations ranging from approximately 12–14% relative to E_{ISO}. This systematic shift suggests that the dynamic approach may capture material response characteristics that are not fully represented in static or quasi-static tests, potentially linked to viscoelastic effects, strain rate sensitivity, or improved filtering of non-linear strain regions.

Notably, variability between specimens within the same group is minimal, with modulus differences between A and B specimens generally below 2%, confirming both reproducibility of the testing protocols and material homogeneity. The largest distinction across groups is observed for P2 specimens, which consistently exhibit lower modulus values than P1 and P3 across all methodologies. This indicates the influence of print direction.

Overall, the comparison highlights that while the ISO 527 standard yields the highest modulus estimates, the regression method provides a more conservative but closely aligned result. The novel dynamic algorithm consistently delivers lower modulus values, yet with excellent repeatability. This suggests potential for the dynamic method as a robust complementary tool, especially in contexts where sensitivity to real-time mechanical response is critical.

6 Discussion

6.1 Overview of Findings

This study systematically investigated the influence of print orientation and extrusion temperature on the tensile properties of FFF-printed PLA. The results clearly demonstrate that both factors have a profound and predictable impact on the final mechanical

performance of the components. Furthermore, the investigation into different calculation methodologies for Young's Modulus has revealed significant discrepancies, highlighting the critical importance of selecting an appropriate analysis technique for generating meaningful engineering data.

6.2 Interpretation of Key Findings

6.2.1 The Critical Role of Print Orientation and Anisotropy

The experimental data unequivocally confirm the anisotropic nature of FFF-printed parts. The vertically oriented specimens (P1) consistently exhibited the highest ultimate tensile strength (UTS) and Young's Modulus. This is because, in this orientation, the tensile load is applied parallel to the extruded filaments (rasters). The primary mode of resistance is the strength of the PLA polymer itself, with minimal stress placed on the weaker interlayer bonds.

Conversely, the horizontally oriented specimens (P2) showed the lowest UTS and were significantly more ductile. Here, the tensile load is applied perpendicular to the layer lines, directly stressing the interlayer adhesion. Failure in these specimens is predominantly due to delamination—the layers pulling apart. The strength is therefore dictated not by the polymer itself, but by the quality of the "weld" between successive layers.

The 45°-oriented specimens (P3) displayed intermediate properties. In this configuration, the applied load is resolved into both shear and normal components relative to the raster lines. This combined stress state results in performance that is superior to the weak interlayer-dominated P2 orientation but inferior to the strong raster-dominated P1 orientation.

6.2.2 The Influence of Extrusion Temperature on Interlayer Adhesion

For every orientation, increasing the extrusion temperature from 210 °C to 220 °C resulted in a measurable improvement in both UTS and stiffness. This phenomenon is directly linked to polymer rheology and interlayer fusion. The higher temperature reduces the viscosity of the molten PLA, promoting better flow and wetting of the previously deposited layer. This enhanced flow allows polymer chains from adjacent layers to intermingle and entangle more effectively before solidification, creating a stronger, more cohesive bond. Essentially, the higher temperature facilitates a better "weld," reducing the size and number of voids at the layer interface and improving the overall structural integrity of the part. This effect is particularly crucial for the P2 and P3 orientations, where interlayer strength is the primary determinant of performance.

6.3 The Discrepancy in Modulus of Elasticity

One of the most significant findings of this study is the substantial difference between the modulus values calculated by the ISO 527 standard and the regression-based and dynamic methods. The regression and dynamic methods consistently produced modulus values 5-14% lower than the standard chord modulus.

The ISO 527 standard calculates the modulus over a very small, early strain range (0.05% to 0.25%). This region is often affected by initial material settling, machine compliance, and the "toe" region of the stress-strain curve, where slack may be removed from the system. Consequently, this method can underestimate the material's stiffness in its true working elastic range.

In contrast, the Dynamically Defined Modulus (Chapter 5) provides a highly robust and objective assessment. By programmatically isolating the largest region of stable stiffness, this method systematically excludes the initial non-linear response and concentrates on the portion of the stress–strain curve that reflects consistent elastic behaviour. Compared to the regression-based approach (Chapter 4), the dynamic method yields slightly lower values, yet the overall trends and relative differences between specimen groups remain highly consistent. This close agreement confirms the validity of both methodologies, while also highlighting that the dynamic approach reduces subjective bias in defining the fitting range. From an engineering perspective, the dynamically defined modulus can be considered a conservative yet reliable estimate of material stiffness. Its consistent

reproducibility across specimens suggests strong potential for use in practical engineering design and FEA simulations, particularly where accurate representation of the material's elastic response under service conditions is required.

6.4 Comparison with Manufacturer-Supplied Data

A comparison between the experimental results and the manufacturer's datasheet reveals interesting points:

- Manufacturer's Elastic Modulus (XY): 1860 MPa
- Highest Measured Elastic Modulus (P1-B, E_{ISO})**:** 1781 MPa

The highest dynamically measured tensile modulus shows remarkable agreement with the manufacturer's flexural modulus for the same orientation. This suggests that for stiff materials like PLA, the two values are closely related when measured under optimal conditions:

- Manufacturer's Tensile Strength (XY): 34.7 MPa
- Highest Measured Tensile Strength (P1-B)**:** 46.34 MPa

The experimentally measured tensile strength in the optimal P1 orientation exceeds the manufacturer's reported value by a substantial margin. This discrepancy is likely due to differences in testing protocols (e.g., ISO 527 in this study versus ASTM or other standards used by the manufacturer), but more importantly, it reflects the highly controlled 3D printing parameters applied here—such as 100% infill, optimized layer height, and precise orientation—which may have produced material properties superior to typical production conditions represented in the datasheet.

6.5 Future work

While this study establishes a crucial baseline using fully solid specimens, the results naturally lead to further avenues of investigation essential for the practical application of FFF printing. Future work should prioritize a systematic analysis of the influence of infill, as parts are rarely printed solid to conserve material and time. Such research should not only quantify the effects of varying infill density on mechanical properties but also explore different geometric patterns. A comparative study of rectilinear, honeycomb, and particularly quasi-isotropic patterns like the gyroid could reveal key strategies for mitigating the directional weakness inherent in the FFF process, allowing for the design of more consistently performing components regardless of load direction.

Beyond process parameters, post-processing techniques present another vital area for future exploration. The properties of a semi-crystalline polymer like PLA can be significantly altered through annealing, a controlled heat treatment process. It is hypothesized that annealing the printed specimens would promote increased crystallinity, leading to greater stiffness and tensile strength. This process would also relieve internal stresses induced during printing, thereby improving dimensional stability. However, it is crucial to also quantify the expected trade-off of decreased ductility, as an increase in strength is often accompanied by a rise in brittleness, a factor that must be considered for parts intended for dynamic or impact-prone applications.

7 Conclusion

This research provided a comprehensive mechanical characterization of FFF-printed PLA, leading to a clearer understanding of how process variables and analysis techniques define a component's final performance. The findings conclusively demonstrate that the inherent anisotropy of the FFF process is the most dominant factor influencing tensile properties. Print orientation dictates whether a load is borne by the strong polymer chains of the extruded rasters or the weaker adhesive bonds between layers, with vertically printed specimens proving consistently stronger and stiffer. Furthermore, it was determined that a modest 10 °C increase in extrusion temperature measurably enhances both strength and stiffness across all orientations by promoting better fusion between layers. Critically, this study also revealed that the chosen method for calculating Young's Modulus significantly impacts the result. The standard ISO 527 chord modulus was found to

overestimate the material's stiffness by 10-15% compared to a more robust, dynamically defined modulus derived from the most stable, linear portion of the material's stress-strain response, which is arguably more representative (and conservative) for practical engineering applications.

In closing, the findings of this research underscore the principle that the properties of an additively manufactured component are not inherent to the material alone but are a complex function of process parameters and characterization methods. It is clear that the path from a spool of filament to a reliable, functional engineering part involves a series of critical decisions. By adopting more robust analysis techniques and continuing to explore the vast parameter space offered by infill strategies and post-processing, the full potential of fused filament fabrication for producing dependable, load-bearing components can be more fully and confidently realized.

Conflicts of Interest: The author(s) report there are no competing interests to declare;

References

[1] I. Gibson, D. Rosen, and B. Stucker, *Additive manufacturing technologies: 3D printing, rapid prototyping, and direct digital manufacturing, second edition*. 2015. doi: 10.1007/978-1-4939-2113-3.

[2] N. Rašović, "Recommended Layer Thickness to the Powder-Based Additive Manufacturing Using Multi-Attribute Decision Support," *Int J Comput Integr Manuf*, vol. 34, no. 5, pp. 455–469, May 2021, doi: 10.1080/0951192X.2021.1891574.

[3] S. Farah, D. G. Anderson, and R. Langer, "Physical and mechanical properties of PLA, and their functions in widespread applications — A comprehensive review," 2016. doi: 10.1016/j.addr.2016.06.012.

[4] A. Rodríguez-Panes, J. Claver, and A. M. Camacho, "The influence of manufacturing parameters on the mechanical behaviour of PLA and ABS pieces manufactured by FDM: A comparative analysis," *Materials*, vol. 11, no. 8, 2018, doi: 10.3390/ma11081333.

[5] V. Slavković, B. Hanželič, V. Plesec, S. Milenković, and G. Harih, "Thermo-Mechanical Behavior and Strain Rate Sensitivity of 3D-Printed Polylactic Acid (PLA) below Glass Transition Temperature (Tg)," *Polymers (Basel)*, vol. 16, no. 11, Jun. 2024, doi: 10.3390/POLYM16111526.

[6] W. D. Callister and D. G. Rethwisch, *Materials science and engineering: an introduction*, 10th ed. Hoboken: Wiley, 2018.

[7] S. H. Ahn, M. Montero, D. Odell, S. Roundy, and P. K. Wright, "Anisotropic material properties of fused deposition modeling ABS," *Rapid Prototyp J*, vol. 8, no. 4, 2002, doi: 10.1108/13552540210441166.

[8] Q. Sun, G. M. Rizvi, C. T. Bellehumeur, and P. Gu, "Effect of processing conditions on the bonding quality of FDM polymer filaments," *Rapid Prototyp J*, vol. 14, no. 2, 2008, doi: 10.1108/13552540810862028.

[9] A. K. Sood, R. K. Ohdar, and S. S. Mahapatra, "Parametric appraisal of mechanical property of fused deposition modelling processed parts," *Mater Des*, vol. 31, no. 1, 2010, doi: 10.1016/j.matdes.2009.06.016.

[10] D. Popescu, A. Zapciu, C. Amza, F. Baciu, and R. Marinescu, "FDM process parameters influence over the mechanical properties of polymer specimens: A review," *Polym Test*, vol. 69, 2018, doi: 10.1016/j.polymertesting.2018.05.020.

[11] A. Lanzotti, M. Grasso, G. Staiano, and M. Martorelli, "The impact of process parameters on mechanical properties of parts fabricated in PLA with an open-source 3-D printer," *Rapid Prototyp J*, vol. 21, no. 5, 2015, doi: 10.1108/RPJ-09-2014-0135.

[12] Y. Zhang and K. Chou, "A parametric study of part distortions in fused deposition modelling using three-dimensional finite element analysis," *Proc Inst Mech Eng B J Eng Manuf*, vol. 222, no. 8, 2008, doi: 10.1243/09544054JEM990.

[13] B. M. Tymrak, M. Kreiger, and J. M. Pearce, "Mechanical properties of components fabricated with open-source 3-D printers under realistic environmental conditions," *Mater Des*, vol. 58, 2014, doi: 10.1016/j.matdes.2014.02.038.

[14] C. Phillips, M. Kortschot, and F. Azhari, "Towards standardizing the preparation of test specimens made with material extrusion: Review of current techniques for tensile testing," *Addit Manuf*, vol. 58, p. 103050, Oct. 2022, doi: 10.1016/J.ADDMA.2022.103050.

[15] M. Mani, T. Murugaiyan, and V. Shanmugam, "Mechanical characterization and puncture resistance of 3D-printed PLA lattice structures," *Polym Eng Sci*, vol. 64, no. 10, pp. 5006–5021, Oct. 2024, doi: 10.1002/PEN.26897.

[16] M. Soldo, "A Newly Modeling Procedure For Different Morphological Distributions Of Unit Cells In Lattice Structure With Constant Relative Density," *International Journal of Innovative Solutions in Engineering*, vol. 1, no. 1, pp. 25–32, Jan. 2025, doi: 10.47960/3029-3200.2025.1.1.25.

[17] V. Plesec, J. Humar, P. Dobnik-Dubrovski, and G. Harih, "Numerical Analysis of a Transtibial Prosthesis Socket Using 3D-Printed Bio-Based PLA," *Materials (Basel)*, vol. 16, no. 5, Mar. 2023, doi: 10.3390/MA16051985.

[18] R. Afshar, S. Jeanne, and B. E. Abali, "Nonlinear Material Modeling for Mechanical Characterization of 3-D Printed PLA Polymer With Different Infill Densities," *Applied Composite Materials*, vol. 30, no. 3, pp. 987–1001, Jun. 2023, doi: 10.1007/s10443-023-10122-y.

[19] ISO, "Plastics – Determination of tensile properties – Part 1: General principles," *527-1*, no. 527–1, 2019.

[20] American Society for Testing and Materials, "ASTM D638-14," *ASTM International*, vol. 82, no. C, 2016.

[21] J. R. C. Dizon, A. H. Espera, Q. Chen, and R. C. Advincula, "Mechanical characterization of 3D-printed polymers," 2018. doi: 10.1016/j.addma.2017.12.002.

[22] I. Krešić, J. Kaljun, and N. Rašovć, "Controlling the Mechanical Response of Stochastic Lattice Structures Utilizing a Design Model Based on Predefined Topologic and Geometric Routines," *Applied Sciences 2024, Vol. 14, Page 6048*, vol. 14, no. 14, p. 6048, Jul. 2024, doi: 10.3390/APP14146048.

[23] ISO 37:2024(en), "Rubber, vulcanized or thermoplastic — Determination of tensile stress-strain properties," Browsing Platform (OBP). Accessed: May 21, 2024. [Online]. Available: https://www.iso.org/obp/ui/en/#iso:std:iso:37:ed-7:v1:en:fig:1